European Journal of Forest Research (2026) 145:33
https://doi.org/10.1007/s10342-026-01875-9

RESEARCH

Understanding tree growth dependencies using multisensorial point clouds

Maryam Poorazimy[1] · Ghasem Ronoud[1,2] · Tuomas Yrttimaa[1] · Ville Luoma[3] · Simone Bianchi[4] · Saija Huuskonen[4,5] · Juha Hyyppä[6] · Ninni Saarinen[1] · Ville Kankare[6,7] · Mikko Vastaranta[1]

Received: 18 March 2024 / Revised: 24 December 2025 / Accepted: 9 January 2026

Abstract
Individual tree crowns are the primary interface with the environment and closely relate to tree growth, yet accurately characterizing them remains challenging. This study aimed to understand how individual tree stem volume growth (ΔV) depends on crown metrics both at the beginning of the monitoring period (T1_C) and on their changes over time (ΔC), using close-range multisensorial point clouds obtained from terrestrial and airborne laser scanning (TLS and ALS). Data were collected from 22 sample plots in boreal forests of Finland in 2014 (T1) and 2021 (T2). Spearman's rank correlation coefficient (ρ) was employed to assess the relationships between ΔV and crown metrics across different tree species. Additionally, Random Forest regression (RF) was applied to explore the relative importance of these metrics in explaining ΔV. A strong correlation (ρ = 0.60–0.63) was found between ΔV of Scots pine (*Pinus sylvestris* L.) and crown metrics, including volume (T1_CV), perimeter (T1_CP), projection area (T1_CA_{2D}), and top height (T1_CH_{max}). In contrast, ΔV of Norway spruce (*Picea abies* (L.) H. Karst.) showed only weak correlations, with the best metrics being crown base height (T1_CH_{min}), T1_CV, and its change (ΔCV) (ρ = 0.32–0.38). For birches (*Betula* sp.), ΔV also exhibited weak correlations (ρ = 0.27–0.34), mainly with crown surface area (T1_CA_{3D}), ΔCV, and T1_CH_{max}. RF analyses further highlighted species-specific drivers of ΔV. Scots pine with the most important metric of T1_CH_{max} explained 50% of variation in ΔV. However, ΔCV was the most important metric in explaining ΔV of Norway spruce and birch, with explained variability of 20% and 6%, respectively. In conclusion, this study demonstrated that multisensorial point clouds provide an effective approach to analyze the relationship between ΔV and tree crown structure. Nevertheless, challenges persist in consistently measuring various crown metrics over time and distinguishing actual changes from measurement errors.

Keywords Terrestrial laser scanning (TLS) · Tree crown · Airborne laser scanning (ALS) · Stem volume · Scots pine · Boreal forests

Introduction

Tree growth is a physio-ecological process that varies both within and between different tree species (Franklin et al. 2002; Coomes and Allen 2007; Pretzsch 2009). Variations in tree growth influences forest stand development, mortality, and the diversity of tree size and spatial patterns (Fraver et al. 2014). Therefore, obtaining information on tree growth is essential for understanding forest ecosystem structure and functioning. Tree growth has been shown to depend on stem size, especially in homogeneous stands (Muller-Landau et al. 2006; Coomes and Allen 2007; Pretzsch 2021). In contrast, heterogeneous stands with a high variation in the shape and size of stems and crowns, require additional information on tree crowns—such as leaf area, crown projection area, crown length, and crown ratio—to explain differences in tree growth (Pretzsch et al. 2015).

Tree crown is vital for growth because it holds the leaves that capture sunlight for photosynthesis (Enquist et al. 2009). The shape and size of the crown also influence water transpiration and gas exchange, which in turn affect overall tree's health and growth rate. Tree crown reflects

Communicated by Tianjian Cao.

Extended author information available on the last page of the article

Published online: 05 February 2026

past growing conditions and interactions between neighboring trees, influencing both the current and future growth of trees (Lüttge and Hertel 2009). Moreover, the temporal and spatial arrangement of tree crowns indicates competition between individuals, ultimately determining how biomass is allocated between foliage and its supporting structure (Weiner 1990, 2004a; Niklas 1994). Thus, a change in the crown structure could lead to a change in the growth allocation strategy and this relationship can vary across different tree species (Weiner 2004a; Vincent and Harja 2008; Harja et al. 2012).

However, traditional methods for measuring crown structure are destructive and labor-intensive. In these methods, trees are felled, and detailed measurements of branch characteristics are conducted to calculate crown structure including the position, length, and angle of branches relative to the initiation point of each annual stem growth unit (Ottorini et al. 1996). Establishing permanent sample plots is also feasible to monitor changes in some of the common individual tree parameters, such as diameter at breast height (dbh) and height (Weiskittel et al. 2011). However, it requires the ability to relocate and remeasure trees which is time-consuming and prone to measurement errors (Luoma et al. 2017).

Terrestrial laser scanning (TLS) is now a widely used technology for non-destructive measurements of trees and forest stands, employing point clouds for the precise reconstruction of their three-dimensional (3D) structure (Calders et al. 2020). The capabilities of TLS in providing the means for measuring tree height and diameters along the stem to estimate a taper curve have been confirmed in both tree and plot-level studies (Vastaranta et al. 2009; Kankare et al. 2014; Liang et al. 2014; Srinivasan et al. 2014; Saarinen et al. 2017; Liu et al. 2018; Yrttimaa et al. 2020a). TLS facilitates the characterization of crown structure, although challenges arise in dense forests where the crowns of individual trees are overlapping (Weiner 2004b; Jung et al. 2011; Metz et al. 2013; Srinivasan et al. 2015). In addition, TLS has demonstrated its capability to monitor tree growth and structural changes if consecutive measurements are collected over time (Sheppard et al. 2017; Luoma et al. 2021; Yrttimaa et al. 2022). However, the below-canopy viewpoint of TLS limits its ability for comprehensive tree characterization due to the reduced visibility of crown structures towards the top of the canopy. These parts of the canopy are often occluded by the crowns of adjacent trees (Liang et al. 2018; Vaglio Laurin et al. 2019; Terryn et al. 2022). In contrast, high-density georeferenced point clouds acquired from above the canopy using an aircraft or an unmanned aerial vehicle (UAV), could provide a complementary viewpoint for TLS measurements and thus benefit the characterization of trees and forests (Yrttimaa et al. 2020b; Terryn et al. 2022). For instance, Yun et al. (2019) showed that the capacity of capturing the leaf area of individual trees using TLS increased from 60 to 73% to 72–90% when supplementary airborne laser scanning (ALS) data was used. Similar results were obtained by Panagiotidis et al. (2022) as they could improve the characterization of the canopy structure for both broad-leaved and coniferous-dominated plots by a fusion of UAV-LS and TLS. Schneider et al. (2019) also suggested using a combination of TLS and UAV-based point clouds for the comprehensive characterization of the canopy at very high spatial resolution (<2% occlusion in estimated canopy volume). However, the combined use of TLS and ALS has not been investigated in change-monitoring applications. Even with multisensorial datasets, repeated measurements over time may be affected by differences in point cloud characteristics between two time points and their spatial alignment. Therefore, assessing consistency of these measurements over time is also necessary to justify the observed changes, while acknowledging the inherent random measurement errors.

Based on the current knowledge, we assume that multisensorial laser scanning data will enhance the monitoring of tree growth compared to relying solely on data obtained from a single sensor. Therefore, the primary aim of this study was to investigate the species-specific relationship between individual tree stem volume growth (ΔV) and crown metrics using bitemporal, multisensorial point clouds including TLS and high-density ALS acquired in 2014 (T1) and 2021 (T2). Both crown metrics at the beginning of the monitoring period (T1_C) and their changes over time (ΔC) were examined. We examined the consistency of multisensorial measurements at T1 and T2 to assess their reliability. Further, the extent to which the crown metrics can explain the variability in ΔV was determined. Based on the observed findings, we discuss the feasibility of using close-range sensing for monitoring the growth dependencies of different tree species within diverse southern boreal forests.

Materials and methods

Study area and field measurements

The study was conducted in the southern boreal forest zone in Evo, Finland (61°19.6′ N 25°10.8′ E, Fig. 1) and included approximately 2,000 ha of managed forest with elevations ranging from 125 to 185 m above sea level. Scots pine (*Pinus sylvestris* L.), Norway spruce (*Picea abies* (L.) H. Karst.), and birch (*Betula* sp.) are the dominant tree species in the study area, contributing 44.7%, 33.5%, and 21.8% of the total volume, respectively. The experimental setup for the current study includes twenty-two field plots with

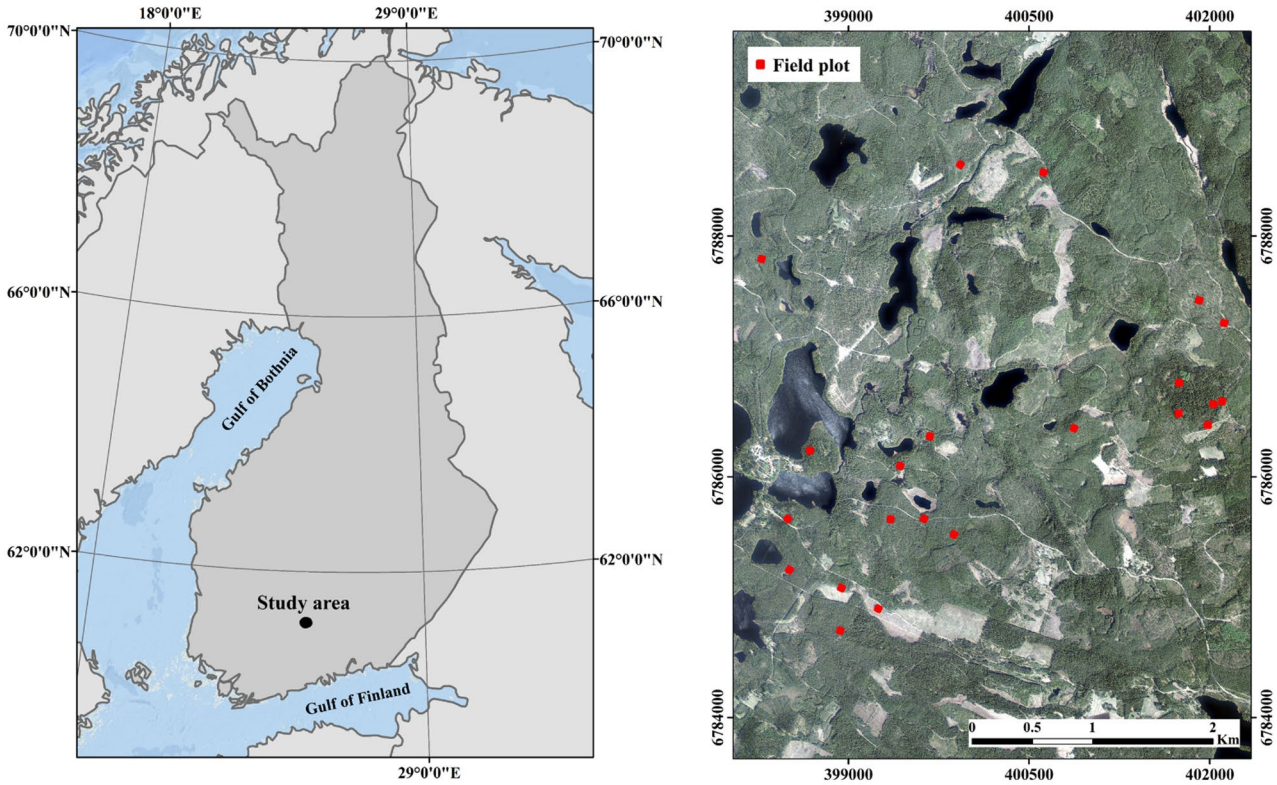

Fig. 1 Location of the study area in Evo, Finland (left) and distribution of field plots overlaid on an orthophoto mosaic acquired in 2022 by the National Land Survey of Finland (right)

Table 1 Summary statistics of field measurements across all 22 plots are presented for the years 2014 (T1) and 2021 (T2)

Attribute	2014				2021			
	Min	Max	Mean	Std.	Min	Max	Mean	Std.
Number of trees (n ha^{-1})	430	3008	1238	731	430	2568	1197	674
Mean volume (m^3 ha^{-1})	110.64	482.33	297.24	115.21	143.89	537.24	356.42	117.14
Basal area-weighted mean dbh (cm)	13.91	41.58	25.93	9.10	16.08	42.41	27.91	8.79
Basal area-weighted mean height (m)	13.03	27.04	21.01	4.14	14.80	28.14	22.50	3.80

The minimum (Min), maximum (Max), mean, and standard deviation (Std.) values for the number of trees and mean stem volume per hectare, along with basal area-weighted mean diameter at breast height (dbh) and height are reported

a fixed size of 32 × 32 m, which were established in 2014 (T1) to support various remote sensing research activities. These sample plots encompass a variety of stand conditions representing different stages of development, species composition, stand density, and canopy layering.

A tree-by-tree field inventory was conducted in the summer of 2014. The attributes recorded for trees with a dbh ≥ 5 cm included tree species, dbh, height, and tree's health status (i.e., dead, or alive). Tree species and health status were assessed based on visual interpretation while measuring dbh with calipers. A Vertex IV clinometer (Haglöf Sweden AB, Långsele, Sweden) was used to measure tree height. Basal area was calculated from the dbh measurements by considering the cross-sectional area of a tree to be circular, and the stem volume was estimated using the nationwide species-specific volume equations with dbh and height as explanatory variables (Laasasenaho 1982). Further, basal area–weighted mean dbh and height were computed by weighting each tree's measurements according to its basal area. The field inventory was repeated in 2021 with remeasuring the dbh and height of all trees that met the predefined dbh threshold. Based on the field inventories, Table 1 presents the number of trees and mean stem volume

per hectare, along with basal area-weighted mean dbh and height for all 22 field plots in 2014 and 2021.

Multisensorial laser scanning data collection

The TLS and high-density ALS datasets were acquired in 2014 (T1) and 2021 (T2) over the study area. Table 2 summarizes the main details of the data acquisition campaigns.

The T1-TLS campaign was conducted in April-May 2014 using a Leica HDS6100 (Leica Geosystems, St. Gallen, Switzerland) phase-shift scanner (Table 2). A total of five individual scans per sample plot were collected to deliver hemispherical point clouds with an angular resolution of 0.018°. There was one scan located at the sample plot center and four auxiliary scans at quadrant directions with an 11.3 m distance around the sample plot center. The point clouds from each sample plot were co-registered and merged using the Z+F LaserControl software. The co-registration of individual scans was implemented using six artificial reference targets attached to the trees, resulting in an average of 2 mm registration accuracy within the sample plot. To create a treemap for each sample plot, the trees were identified and located through visual detection of stem-cross sections from a horizontal slice of the T1-TLS points cloud. The treemaps were verified in the field, and any undetected trees were located during the tree-by-tree inventory.

A Leica RTC360 3D time-of-flight scanner was used for the T2-TLS campaign conducted in April-May 2021 (Table 2). A multi-scan approach was implemented to deliver a hemispherical points cloud with an angular resolution of 0.009° while the scan setup was modified from that applied in T1 by placing eight auxiliary scans approximately at plot borders in addition to the central scan. The same co-registration procedure with a similar level of accuracy was applied to the T2-TLS point clouds using a Leica Cyclone 3D Point Cloud Processing Software. The existing treemaps were also updated with the trees that had reached the measurement threshold (i.e., dbh ≥ 5 cm). Respectively, the trees that had been harvested or fallen during the monitoring period were removed from the tree maps.

The T1-ALS data was acquired using a RIEGL VQ-480-U scanner (RIEGL Laser Measurement Systems GmbH, Austria) mounted on a helicopter in December 2014 (Table 2). The scanner was a lightweight pulsed scanner with a beam divergence of 0.3 mrad. It was operated at a 550-kHz pulse repetition rate with a flight height of approximately 75 m above the ground level. The target flight speed was 50 km/h and point clouds with a density of 450 pts/m^2 were produced with a point spacing of 4.7 cm on the ground.

A multi-sensorial system carried by a helicopter was used to collect the T2-ALS data in June 2021 including three Riegl laser scanners of VUX-1HA, MiniVUX-3UAV, and VQ-840-G (Table 2). The pulse repetition rate was 1017, 300, and 200 kHz for the mentioned sensors respectively at a target flying speed of 50 km/h. The flight height was approximately 80 m above the ground level resulting in a point density of 3200 pts/m^2 and a point spacing of 2.0 cm on the ground.

Table 2 Acquisition setup of multisensorial datasets including terrestrial laser scanning (TLS) and close-range airborne laser scanning (ALS) in 2014 (T1) and 2021 (T2)

Specification	2014		2021	
	TLS	ALS	TLS	ALS
Sensor	Leica HDS6100	Riegl VQ 480-U	Leica RTC360 3D	Riegl VUX-1HA/ Mini-VUX-3UAV/ VQ-840-G
Wavelength	690 nm	1550 nm	1550 nm	1550/905/532 nm
Beam divergence	0.22 mrad	0.3 mrad	0.16 mrad	0.5/0.5 × 1.6/1 mrad
Field of view	310° vertically and 360° horizontally	60°	300° vertically and 360° horizontally	360°/120°/40°

Pre-processing multisensorial laser scanning point clouds and co-registration

The T1-TLS point clouds were first co-registered to a global coordinate system of EUREF-FIN based on the location of artificial reference targets, ensuring spatial alignment of the datasets (Fig. 2). To accomplish this, at least two reference points were located on open areas either inside or outside the plots using a Trimble R8 GNSS receiver (Trimble Inc., CA, USA) with a real-time kinematic (RTK) correction. A survey point was also established near the plot center using distance and angle from the reference points. Finally, the location of artificial reference targets was determined using a Trimble 5602 DR200+total station. The manual co-registration was applied by determining whether the T1-TLS and T1-ALS point clouds overlapped from top and side views and further fine-tuned if discrepancies between the T1-TLS and T1-ALS point clouds in the horizontal plane persisted. For characterizing individual trees, a standard height-normalization procedure was applied for the TLS and ALS point clouds (Fig. 2). To accomplish this, point clouds were first classified into ground and non-ground points and then normalized by transforming the Z-coordinate relative to the height above the ground surface using the LAStools software (Rapidlasso 2023). This was followed by the co-registration of the local TLS with georeferenced ALS point clouds at T2 (Fig. 2).

Co-registration of the T2-TLS was carried out by searching for correspondent structures from the T2-ALS data. The

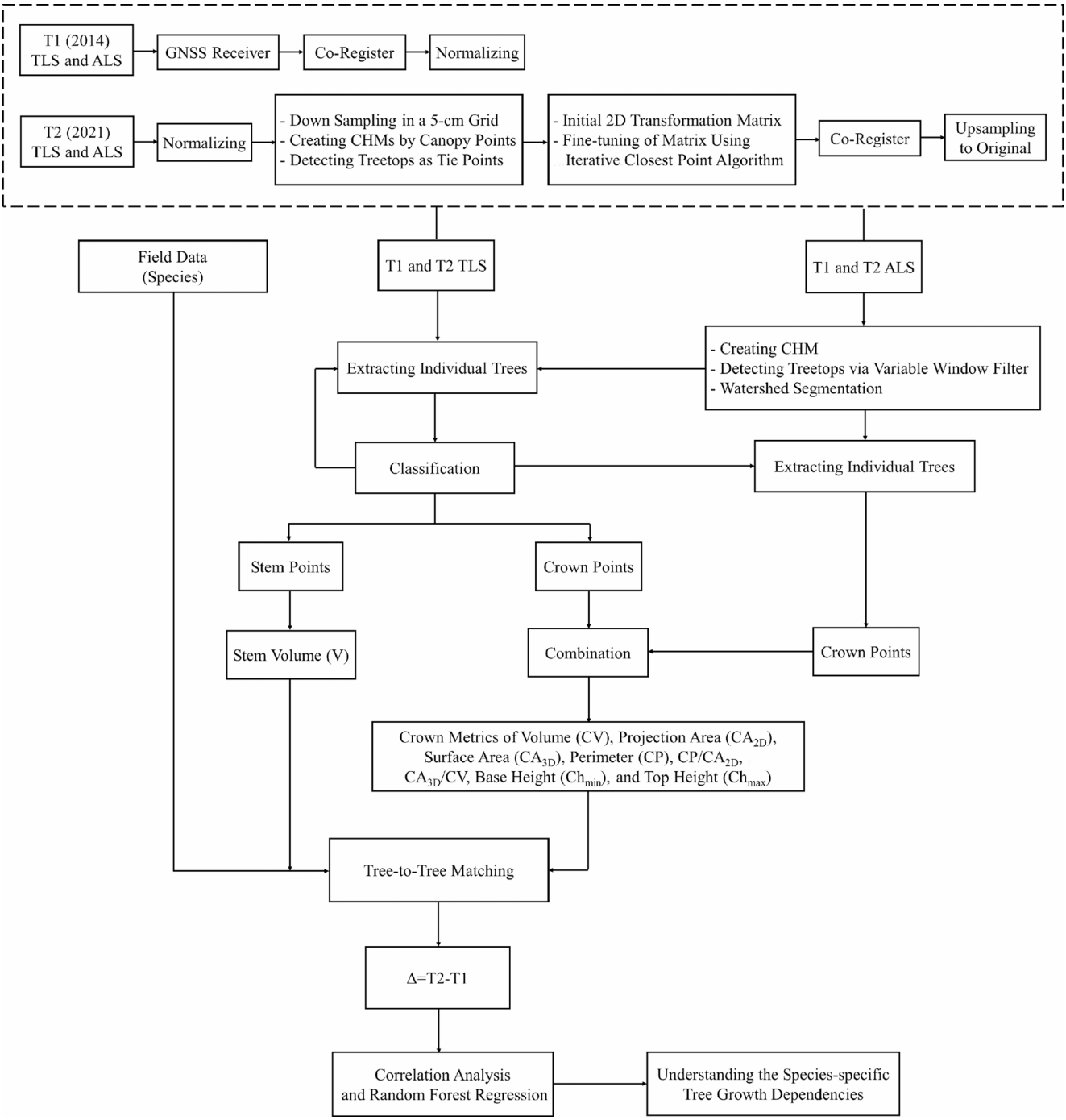

Fig. 2 The workflow of applied methodology. TLS stands for terrestrial laser scanning, ALS for airborne laser scanning, GNSS for global navigation system, and CHM for canopy height model

workflow was similar to that initially presented by Dai et al. (2019) and was adopted to align the normalized TLS and ALS point clouds. First, points obtained above 60% of the maximum height of each sample plot point cloud from both T2-TLS and T2-ALS were considered as canopy points. Those canopy points were then down-sampled into a 5-cm grid to ensure comparable point cloud characteristics such as point spacing between the datasets. Second, the canopy height models (CHMs) were generated from the identified canopy points for both T2-TLS and T2-ALS (i.e., CHM_{TLS} and CHM_{ALS}) using a 40 cm grid. The CHMs were further used to find the locations of treetops by applying local maxima filtering (LMF) with a variable window size (Pitkänen et al. 2004). Third, the XY locations of the treetops

considered as canopy tie points were used to estimate the initial 2D rigid transformation matrix between T2-TLS and T2-ALS. This included XY-translation and rotation along the Z-axis. The transformation solution was then fine-tuned using the Iterative Closest Point (ICP) algorithm applied on the sampled canopy points (Zhang 1994). Using the final 2D rigid transformation matrix, the T2-TLS and T2-ALS could be co-registered with accuracy better than 10 cm. In this context, such accuracy ensured that combining TLS and ALS data did not artificially expand the horizontal extent of tree crowns but rather enhanced the vertical reconstruction of the point clouds, as intended (Fig. 3).

Extraction of individual trees from the multisensorial laser scanning point clouds

The point cloud processing workflow initially presented in Yrttimaa et al. 2019, 2020a) was applied in this study (Fig. 2). The workflow began with a preliminary individual tree segmentation to delineate the sample plot point cloud into reasonable processing units and was followed by semantic point cloud classification aiming at separating points originating from the stem and crown of individual trees. This workflow was applied separately for T1 and T2 point clouds. A marker-controlled watershed segmentation was used to generate individual tree crown segments (Meyer and Beucher 1990) from the ALS CHM that was expected to better represent the upper canopy structure. For this purpose, ALS CHMs were first generated from the height-normalized ALS point clouds at a 40 cm resolution. The treetops identified as local maxima in the CHMs using a Variable Window Filter approach (VWF) (Popescu and Wynne 2004) were then used as the markers in the watershed segmentation. The derived crown segments for individual trees were used to determine a set of ALS and TLS points belonging to each tree (or a group of trees with mixed crowns) using a point-in-polygon approach. In cases where multiple stems were later distinguished within a crown segment, a Voronoi diagram was used to split the point cloud segment accordingly. Individual tree-segmented TLS point clouds were then classified into stem and crown points based on point neighborhood characteristics assuming stem points have more planar, vertical, and cylindrical characteristics than points representing branches and foliage (Fig. 4) (Yrttimaa et al. 2020a). This was accomplished by binning the data into horizontal slices with a repetitive procedure carried out for each slice. This included downsampling (voxelization) the point cloud into a 5 mm regular grid, computation of surface normal vectors for each point based on a plane defined by 40 neighbor points to reveal smooth and vertical surfaces, and clustering those with a minimum 30 cm Euclidian distance from each other, with

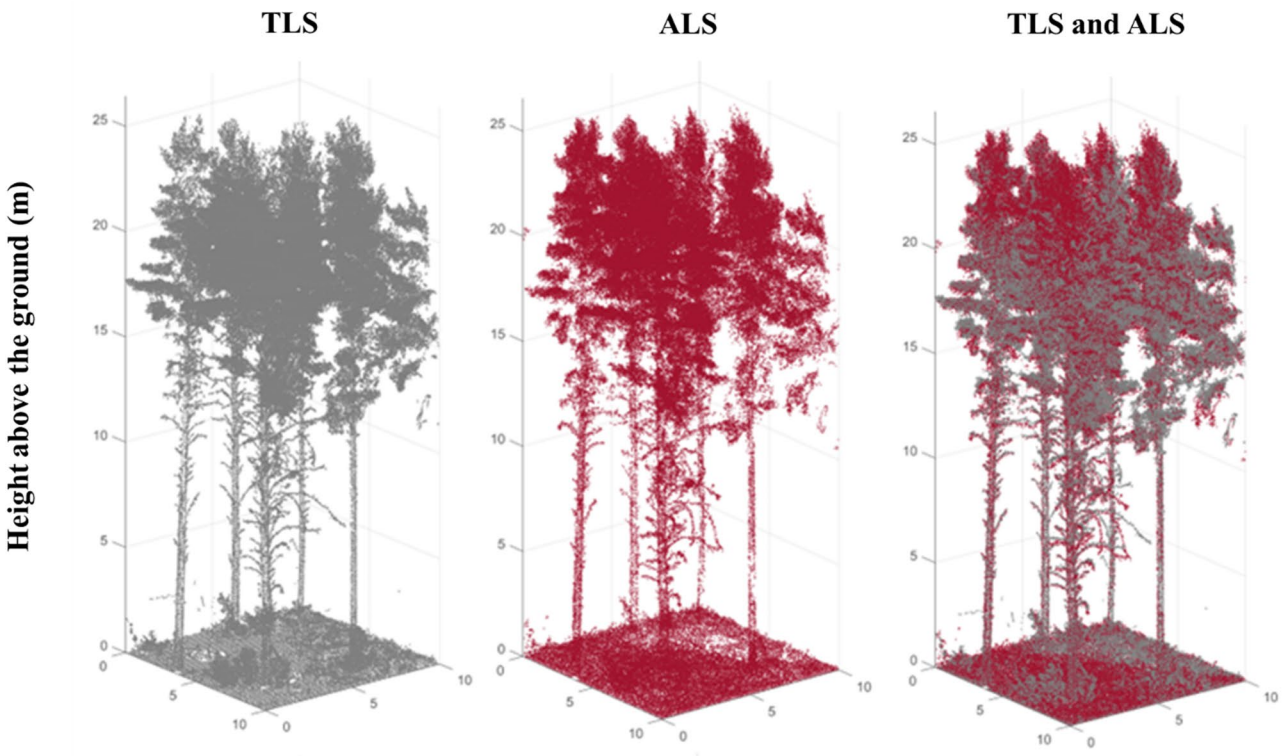

Fig. 3 A sub-sample of normalized point clouds representing terrestrial laser scanning (TLS), high-density airborne laser scanning (ALS), and co-registered TLS and ALS

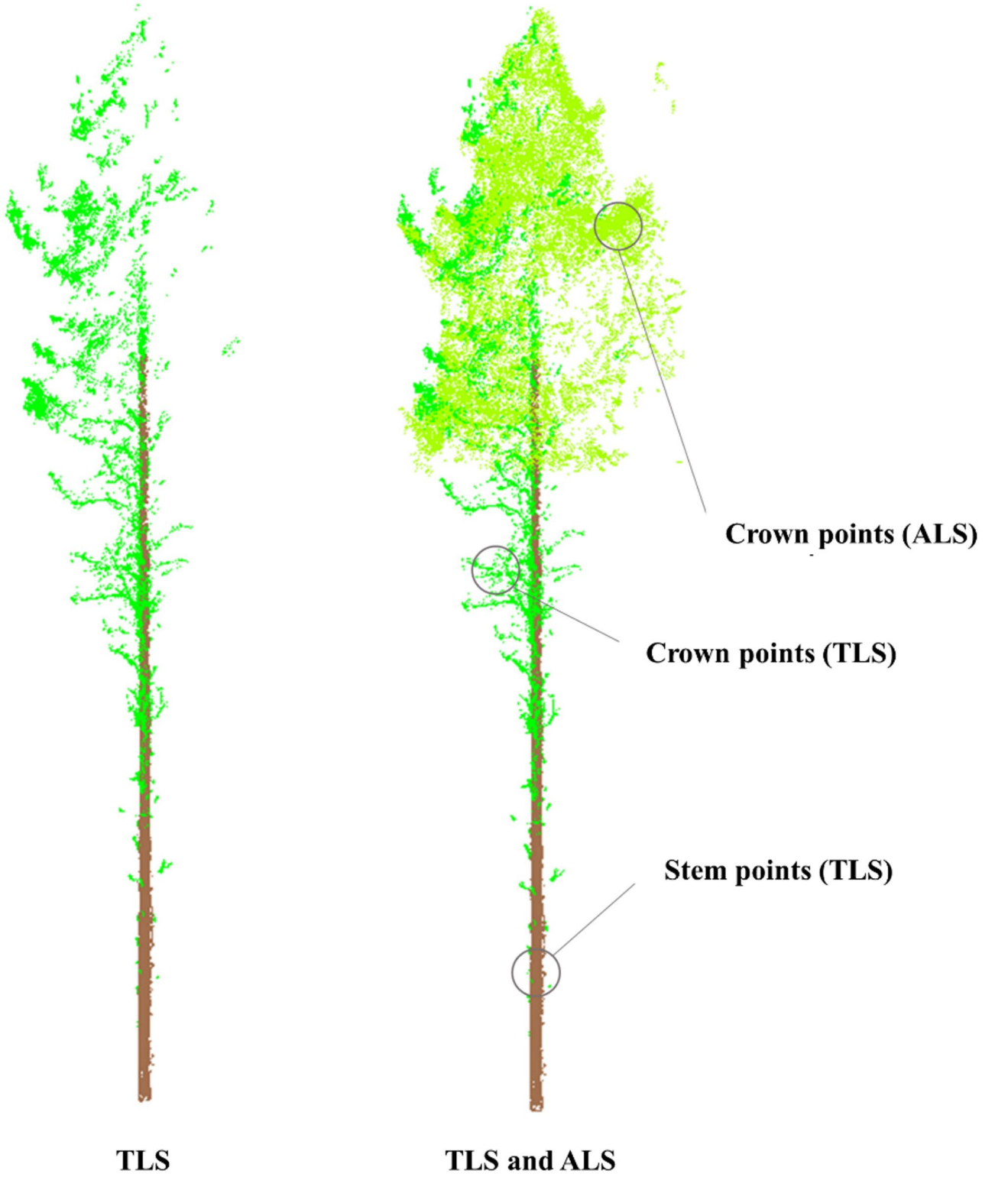

Fig. 4 An illustration of terrestrial laser scanning (TLS) point clouds depicting an individual tree with points originating from the stem separated from points originating from the crown (left), augmented with a high-density airborne laser scanning (ALS) point clouds to provide a complete characterization of the tree crown structure (right)

small and horizontal clusters being filtered out. Then, a random sample consensus (RANSAC)-cylinder filtering was applied, aiming at removing points that deviated from the cylindrical form of the recognized tree stem. Once this procedure was repeated through all the horizontal point cloud slices, TLS points considered to represent the stem surface were enveloped with an alpha shape, and all TLS and ALS points falling outside of the shape were considered to represent the crown (i.e., TLS crown points and ALS crown points; Fig. 4). The XY location of a RANSAX cylinder fitted at breast height was considered a tree location.

Characterizing individual trees and their change using the multisensorial laser scanning point clouds

The TLS points labeled as 'stem points' were used for computing the individual tree stem volume (V) at T1 and T2 (Fig. 2). We followed the procedure originally developed by Yrttimaa et al. (2019) to estimate the taper curve i.e., stem diameter as a function of tree height. First, the stem points were binned into horizontal slices at 20 cm vertical intervals (starting from 1.30 m above the ground and moving towards the stump and treetop, respectively) and the tree diameters were measured by circle fitting at those intervals. Second, outliers in diameter-height observations were removed based on the method initially presented by Saarinen et al. (2017). Finally, a cubic spline curve with a smoothing parameter of 0.5 was fitted into the diameter-height observations for leveling unevenness, interpolating missing values, and obtaining the taper curve at 10 cm intervals up to the top of the tree. Considering the stem as a sequence of vertical cylinders at predefined sections in 10 cm height intervals, the Huber formula (Eq. 1) was used to estimate V based on the estimated taper curve (Table 3).

$$V = \sum_{i=1}^{n} \frac{\pi h_i}{16}(d_i + d_{i+1})^2 \quad (1)$$

where h_i and d_i are the height and diameter of cylinder i respectively, and n is the total number of cylinders. The growth in individual tree stem volume (ΔV) was obtained by subtracting the TLS-derived V in T1 from its respective measure at T2.

The TLS points labeled as 'crown points' were combined with the respective ALS-derived crown points to obtain a comprehensive reconstruction of tree crowns (Fig. 2). The combined data was used to quantify crown characteristics by applying geometry calculation including 2D and 3D convex hulls, and voxel-based approaches (Table 3) (Fernández-Sarría et al. 2013; Yrttimaa et al. 2022). The 2D projection area (CA_{2D}) and perimeter (CP) were obtained by identifying points lying on a 2D convex hull. Crown surface area (CA_{3D}) was estimated using a 3D convex hull by applying Delaunay triangulations to the outer points of the closed convex surface boundary. Given the high density of combined data including redundant points, the crown volume (CV) was computed by voxelizing the points into a 10-cm regular 3D grid (Yan et al. 2019). As a measure of how efficiently a tree utilizes resources to achieve a certain architectural structure, the perimeter-to-projection area ratio (CP/CA_{2D}) and surface area-to-volume ratio (CA_{3D}/CV) were calculated (Yrttimaa et al. 2022). These metrics are useful to understand crown shape as a tradeoff between photosynthetic gain and maintenance cost. It is worth mentioning that the need for capturing light is the key to tree crown development in certain shapes (Seidel et al. 2019). Hence, a lower CP/CA_{2D} indicates a tree that achieved a larger area with less perimeter, potentially leading to better crown architecture in terms of light capture and maintenance cost. Similarly, CA_{3D}/CV is the ratio between the crown surface in the cost of its volume and larger ratios potentially mean more optimized architectures. The crown base height (CH_{min}) and top height (CH_{max}; representing tree height) were two other metrics representing the lowest point of the 3D convex hull

Table 3 Description of metrics characterizing tree and crown derived from TLS and a combination of TLS and ALS, respectively

Metric	Abbreviation (unit)	Description
Stem volume	V (dm^3)	Calculated by considering the stem as a sequence of vertical cylinders (Eq. 1).
Crown volume	CV (m^3)	Calculated as the sum of the volumes of 0.1 m voxels occupied by crown points.
Crown projection area	CA_{2D} (m^2)	The area of a 2D convex hull enveloping crown points projected onto the XY plane.
Crown surface area	CA_{3D} (m^2)	The area of a 3D convex hull enveloping crown points.
Crown perimeter	CP (m)	The perimeter of a 2D convex hull enveloping crown points.
Crown perimeter-to-projection area ratio	CP/CA_{2D} (m/m^2)	The ratio of CP to CA_{2D}.
Crown surface area-to-volume ratio	CA_{3D}/CV (m^2/m^3)	The ratio of CA_{3D} to CV.
Crown base height	CH_{min} (m)	The height at which the 3D convex hull enveloping crown points reaches its lowest points.
Crown top height	CH_{max} (m)	The highest point within the crown segment, corresponding to tree height.

Metrics were extracted at two time points, 2014 (T1) and 2021 (T2). The change in each metric over the monitoring period was then calculated by Subtracting T1 measures from the respective T2 measures (Δ = T2–T1)

and the highest point within the crown segment, respectively (Table 3). These crown metrics describe the crown at T1 (T1_C) and T2 (T2_C). To compute the change in crown metrics during the monitoring period (ΔC), T1_C obtained by ALS and TLS combination were subtracted from the respective T2_C, resulting in ΔCA_{2D}, ΔCV, ΔCA_{3D}, ΔCP, $\Delta(CP/CA_{2D})$, $\Delta(CA_{3D}/CV)$, ΔCH_{min}, and ΔCH_{max} estimates. The T1_C together with ΔC were later used in the analysis.

Individual tree-to-tree matching

To quantify the species-specific changes over time, tree-to-tree matching was required for linking field-measured and point cloud-based observations. In this study, the species information of the extracted individual trees was obtained by searching for the corresponding field-measured tree for each T1-TLS-measured tree, applying a 1.5-m search radius. A similar, XY location-based search was also applied to link the T1-TLS measurements with the T2-TLS measurements. In both scenarios, if multiple candidates were found within the search radius, similarity in the tree metrics was considered to confirm the match between the field measurements and T1-TLS measurements as well as between the T1-TLS and T2-TLS measurements. In addition, to target the analysis on trees with sufficient point cloud reconstruction at both T1 and T2, we accepted following thresholds for tree metric variability between the subsequent measurements: difference in the field-measured and TLS-derived dbh < 3 cm, difference in TLS derived diameter at 6 m height < 4 cm, difference in TLS-derived crown volume < 70%, and difference in TLS-derived tree height < 6 m. These threshold values were determined based on experiences of the TLS-based tree characterization accuracy and its variability within the sample plots. The matched trees carrying their species information were further grouped by tree species: Scots pine, Norway spruce, and birch. After removing outliers which were three times the interquartile range larger than the first and third quartile of ΔV, 219 Scots pine, 112 Norway spruce, and 77 birch trees were used in the analysis. Summary statistics for the matched trees measured in the field plots are provided in Table 4.

Analyzing the capability of multisensorial point clouds to understand species-specific tree growth dependencies

To evaluate the reliability of measurements derived from bitemporal, multisensorial point clouds, we initially assessed their consistency between T1 and T2 using Pearson's correlation coefficient (r) and visual inspection through scatterplots. This analysis aimed to provide justification for observing changes in tree and crown structures using applied methodologies. A high agreement between the T1 and T2 measures of the same attribute would imply consistency in the measurements. Such consistency suggests that the observed variations may reflect a real change in the investigated tree and crown metrics, while acknowledging the inherent random measurement errors.

Subsequently, the monotonic relationships between ΔV and crown structural metrics at T1, as well as their ΔC were explored employing Spearman's rank correlation coefficient (ρ) as a measure of the strength of association. This analysis was intended to provide an initial understanding of species-specific relationships between individual metrics and ΔV, independent of interactions. The statistical significance of the observed relationships was confirmed according to the associated p-value considering a 95% confidence interval.

Table 4 Summary statistics of matched trees by tree species, derived from field measurements/point clouds, are presented for the years 2014 (T1) and 2021 (T2)

Attributes/Species group		Scots pine (n = 219)		Norway spruce (n = 112)		Birch (n = 77)	
		2014	2021	2014	2021	2014	2021
Dbh (cm)	Min	5.45/4.91	5.20/4.86	6.35/4.65	6.20/5.09	6.50/7.26	6.45/6.66
	Max	57.10/54.40	58.60/56.33	50.70/48.75	54.00/50.25	29.75/31.84	32.50/32.52
	Mean	19.10/18.93	20.76/20.10	21.54/21.90	23.04/22.77	16.60/16.74	18.10/17.64
	Std.	7.77/7.48	8.36/7.86	10.02/9.78	10.43/10.02	5.63/5.56	6.04/5.95
Stem volume (m^3)	Min	0.01/0.01	0.01/0	0.01/0.01	0.01/0	0.01/0.03	0.01/0.01
	Max	3.34/3.12	3.87/3.35	2.78/3.07	3.38/3.30	0.77/0.96	1.02/0.95
	Mean	0.31/0.32	0.40/0.38	0.52/0.57	0.62/0.65	0.24/0.26	0.31/0.28
	Std.	0.37/0.35	0.44/0.40	0.51/0.57	0.59/0.63	0.20/0.21	0.24/0.23
Height (m)	Min	5.80/7.59	6.00/10.31	5.30/8.06	5.40/9.92	7.60/9.58	7.10/11.55
	Max	34.30/34.14	36.00/34.57	34.40/34.85	37.40/35.84	29.70/25.89	29.50/28.59
	Mean	16.75/17.00	18.75/19.01	19.74/23.90	21.23/25.41	19.18/18.90	20.76/21.03
	Std.	4.65/4.37	5.09/4.33	7.49/4.78	7.70/4.53	4.66/3.77	4.81/3.87

The minimum (Min), maximum (Max), mean, and standard deviation (Std.) of the diameter at breast height (dbh), stem volume, and height are reported

These analyses were applied across different tree species to determine species-specific relationships.

To further explain these species-specific relationships, we employed a random forest (RF) model. The RF allowed us to assess the potential non-linearity in these relationships, particularly considering the distribution of ΔV. Moreover, this model is well-suited to handle complex interactions between predictors and can manage collinearity to some extent, due to its ensemble structure of decision trees (Breiman 2001).

The entire sample size was used to build the RF model as the goal was to maximize the use of available data to uncover tree growth dependencies. Hence, we ensured the model reflected all the variability present. To address collinearity among crown metrics, the highest-correlating metrics with $r > 0.8$ were retained, while their most redundant counterparts were eliminated. This step ensured that the predictors included in the RF model were not overly correlated, reducing the risk of multicollinearity affecting the model's performance.

The Gini index was then employed to compute the relative importance of the selected predictors. It quantifies the extent to which the metrics contribute to reducing the impurity of decision tree nodes (Hapfelmeier et al. 2014), and the resulting values were scaled into a range of 0-100 for a more intuitive comparison. To facilitate the interpretability of the RF models, we used partial dependence plots to gain more detailed insight into the species-specific relationships between the most important predictors and ΔV in the RF model while other metrics were kept constant (Greenwell 2017).

Finally, the coefficient of determination (R^2) was used to quantify the proportion of observed variation in ΔV that could be explained by crown structure and its ΔC, allowing an assessment of the overall strength of the relationship by tree species (Eq. 2).

$$R^2 = \frac{\sum_{i \in n} (y_i - \hat{y})^2}{\sum_{i \in n} (y_i - \bar{y})^2} \quad (2)$$

where $\hat{y}_i$ is the predicted value, y_i is the observed value, $\bar{y}$ is the mean of observed values, and n is the sample size.

Results

Consistency of species-specific point clouds over the monitoring period

Figure 5 shows the relationship between individual tree characteristics measured in T1 and T2, including V and crown metrics. CH_{max} demonstrated the most consistent change over time, with an $r > 0.97$. Following that, CV was increased through time with correlations of 0.85 for the Scots pine, 0.82 for the Norway spruce, and 0.74 for the birch trees, showing some variability among individual trees. The other crown metrics exhibited more variability around the 1:1 line (Fig. 5). CH_{min} is an example where its variation was likely associated with measurement errors. The lowest consistency was observed for CA_{3D}/CV in Scots pine, Norway spruce, and birch trees with correlations of 0.65, 0.56, and 0.40, respectively. For other metrics, birch trees were found to have higher variability than Scots pine and Norway spruce, with a maximum correlation of 0.81 for the CA_{2D} (Fig. 5). For CA_{2D}, CA_{3D}, and CP, Norway spruce trees showed a higher correlation than pine trees ($r > 0.90$).

The highest correlation was observed for the V ($r > 0.97$) (Fig. 5). Further investigation of estimated ΔV for three different species showed a right-skewed distribution, especially for pine and spruce (Fig. 6). The ΔV mean values were 62.60, 77.57, and 28.83 dm^3 for pines, spruces, and birches, respectively.

The correlation between stem volume growth (ΔV) and crown metrics

For the Scots pine trees, T1_CV, T1_CP, T1_CA_{2D}, and T1_CH_{max} were the metrics with the highest positive correlations (ρ = 0.60–0.63), all statistically significant at a 95% confidence interval. The T1_CP/CA_{2D} demonstrated a negative relationship with Scots pine ΔV, with an ρ of − 0.59. Additionally, T1_CA_{3D} with $\rho = 0.58$ and ΔCV with $\rho = 0.53$ showed a strong positive correlation with Scots pine ΔV (p-value < 0.001). The metrics of T1_CV and T1_CH_{min} were among the highest correlated metrics with Norway spruce ΔV with ρ of 0.38 and 0.34, respectively (p-value < 0.001). Following that, T1_CA_{3D}/CV, and ΔCV exhibited correlation of 0.32 at a 95% confidence interval. Birch ΔV had the highest correlation with ΔCV, reaching a value of $\rho = 0.34$ (p-value < 0.01). In comparison, metrics of T1_CH_{max}, T1_CA_{3D}, and T1_CA_{2D} showed a lower correlation with birch ΔV (ρ = 0.25–0.28, p-value < 0.05). Table 5 shows the monotonic relationships between various crown metrics and ΔV for three species groups of Scots pine, Norway spruce, and birch.

Explaining species-specific stem volume growth (ΔV) using crown metrics

Using crown structural metrics and their ΔC in the RF model, we were able to explain 50% of the variation in Scots pine ΔV ($R^2 = 0.50$) (Fig. 7). For Norway spruces, the explained variation in ΔV was 20%, a notably lower

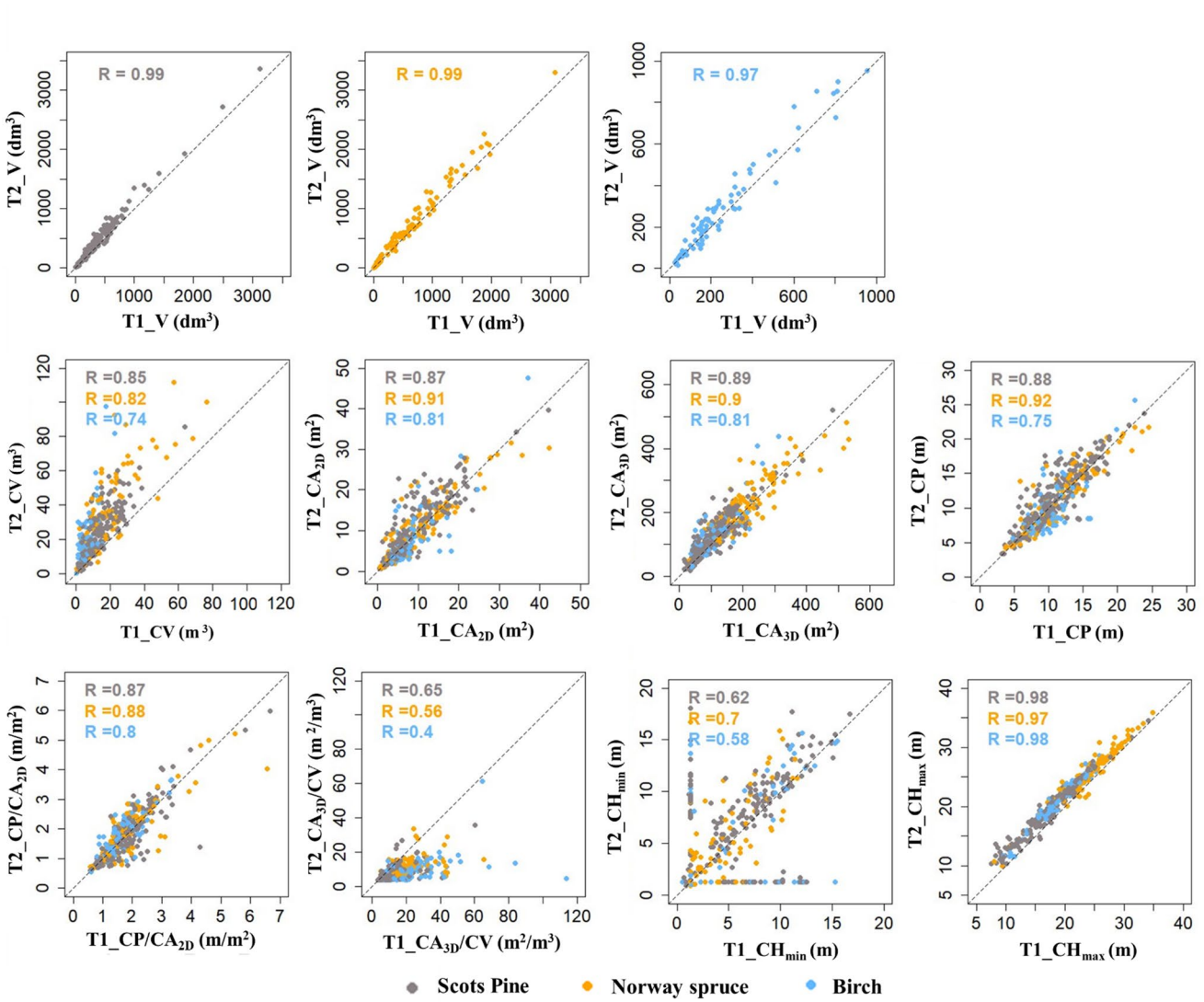

Fig. 5 Scatter plots and Pearson's correlation coefficient (*r*) visualize the consistency of species-specific individual tree characteristics measured in T1 (2014) and T2 (2021). These characteristics include individual tree stem volume (V) and the following crown metrics: volume (CV), 2D projection area (CA_{2D}), surface area (CA_{3D}), perimeter (CP), perimeter to projection area ratio (CP/CA_{2D}), surface area to volume ratio (CA_{3D}/CV), base height (CH_{min}), and top height (CH_{max})

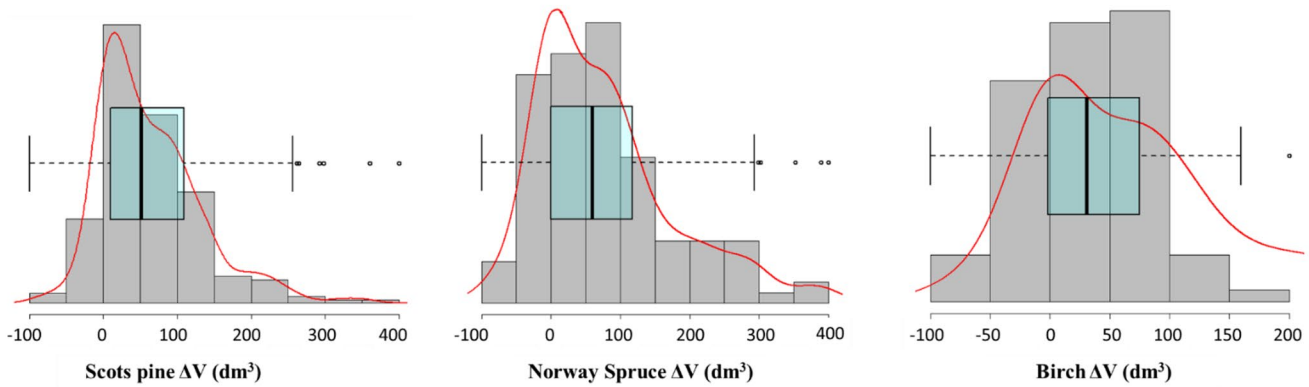

Fig. 6 The distribution of individual tree stem volume growth (ΔV) for Scots pine, Norway spruce, and birch trees is illustrated in the histogram and box plots. The red line represents the density curve

Table 5 Spearman's rank correlation coefficients measuring the relationship between stem volume growth (ΔV) and various crown metrics at T1 (T1_C) as well as their changes (ΔC)—including volume (CV), 2D projection area (CA_{2D}), surface area (CA_{3D}), perimeter (CP), perimeter to projection area ratio (CP/CA_{2D}), surface area to volume ratio (CA_{3D}/CV), base height (CH_{min}), and top height (CH_{max})—are provided

Crown metrics	Scots pine		Norway spruce		Birch	
	Correlation	*p*-value	Correlation	*p*-value	Correlation	*p*-value
T1_CV	0.63^{ab}	$2.01e-25^{***}$	0.38^{abc}	$4.49e-05^{***}$	0.24	$3.27e-02^{*}$
$T1\_CA_{2D}$	0.62^{ac}	$0.00e+00^{***}$	0.28^{ade}	$3.33e-03^{**}$	0.25^{a}	$2.69e-02^{*}$
$T1\_CA_{3D}$	0.58	$0.00e+00^{***}$	0.27^{bdf}	$3.98e-0.3^{**}$	0.27	$1.69e-02^{*}$
T1_CP	0.63^{bcd}	$0.00e+00^{***}$	0.30^{cef}	$1.58e-03^{**}$	0.25^{ab}	$2.66e-02^{*}$
$T1\_CP/CA_{2D}$	-0.59^{d}	$0.00e+00^{***}$	−0.26	$6.25e-03^{**}$	-0.22^{b}	$5.40e-02^{ns}$
$T1\_CA_{3D}/CV$	−0.36	$6.04e-08^{***}$	-0.32^{g}	$5.08e-04^{***}$	-0.05^{c}	$6.64e-01^{ns}$
$T1\_CH_{min}$	0.38	$9.47e-09^{***}$	0.34	$2.82e-04^{***}$	0.10	$3.76e-01^{ns}$
$T1\_CH_{max}$	0.60	$5.46e-23^{***}$	0.29	$1.70e-03^{**}$	0.28	$1.37e-02^{*}$
ΔCV	0.53	$3.76e-17^{***}$	0.32	$5.57e-04^{***}$	0.34	$2.67e-03^{**}$
ΔCA_{2D}	0.25^{e}	$1.63e-04^{***}$	0.19^{h}	$4.81e-02^{*}$	0.10^{d}	$4.12e-01^{ns}$
ΔCA_{3D}	0.19	$4.33e-03^{**}$	−0.003	$9.73e-01^{ns}$	0.02	$8.43e-01^{ns}$
ΔCP	0.17^{e}	$1.00e-02^{*}$	0.19^{h}	$4.26e-02^{*}$	0.16^{de}	$1.77e-01^{ns}$
$\Delta(CP/CA_{2D})$	−0.23	$7.89e-04^{***}$	−0.21	$2.92e-02^{*}$	-0.11^{e}	$3.93e-01^{ns}$
$\Delta(CA_{3D}/CV)$	0.04	$5.39e-01^{ns}$	0.13^{g}	$1.70e-01^{ns}$	-0.10^{c}	$4.31e-01^{ns}$
ΔCH_{min}	0.16^{f}	$1.83e-02^{*}$	0.15^{i}	$1.18e-01^{ns}$	0.18^{f}	$1.28e-01^{ns}$
ΔCH_{max}	0.21^{f}	$1.62e-03^{**}$	0.14^{i}	$1.37e-01^{ns}$	0.15^{f}	$1.91e-01^{ns}$

Significance level denoted as ^{ns} (not significant) for *p*-value > 0.05, * for *p*-value < 0.05, ** for *p*-value < 0.01, and *** for *p*-value < 0.001. Metrics sharing the same superscript letter represent collinear pairs

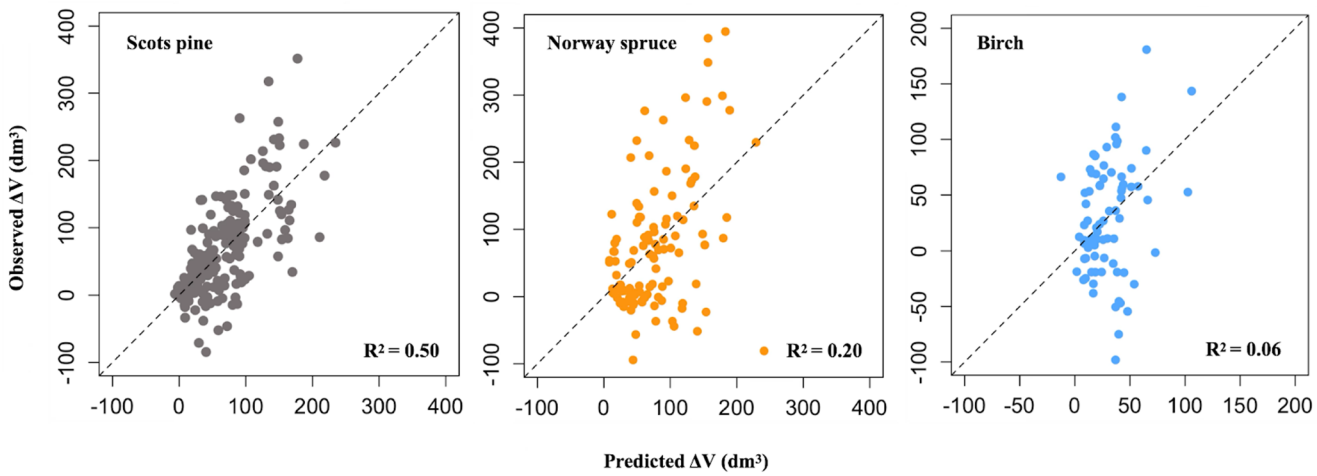

Fig. 7 Scatter plot depicting observed versus predicted stem volume growth (ΔV) of Scots pine, Norway spruce, and birch trees. The dashed line represents the 1:1 relationship

proportion compared to Scots pine trees (Fig. 7). Only 6% of the ΔV variation was explained by the crown structural metrics in birch trees (Fig. 7).

According to the scaled mean decrease in the Gini Index, $T1\_CH_{max}$ was the most important metric in determining Scots pine ΔV (Fig. 8). T1_CP also contributed to the Scots pine ΔV predictions with a relative importance of 44.16. Based on the partial dependence plots, an increase in both $T1\_CH_{max}$ and T1_CP increased the predicted ΔV of Scots pine (Fig. 8a and c). Even though $T1\_CP/CA_{2D}$ demonstrated a rather high relative importance of 45.09 in the RF model, the partial dependence plot showed that there is only a small range of values where the changes in $T1\_CP/CA_{2D}$ affected the predicted ΔV of Scots pine (Fig. 8b). $T1\_CA_{3D}$ with a relative importance of 29.22, is another metric with a notable impact on the predicted Scots pine ΔV (Fig. 8). The predicted ΔV of Scots pine increases as the $T1\_CA_{3D}$ increases up to 280 m^3 while showing no discernible effect beyond that (Fig. 8d). Additionally, ΔCV and ΔCA_{2D} were among the selected predictors that contributed to predicting Scots pine ΔV, even though to a lesser extent. Their relative importance was 27.00 and 20.04, respectively.

The most important metric for explaining Norway spruce ΔV was ΔCV (Fig. 9). The partial dependence plot showed that an increase in ΔCV was associated with an increase in predicted Norway spruce ΔV (Fig. 9a). Likewise, the

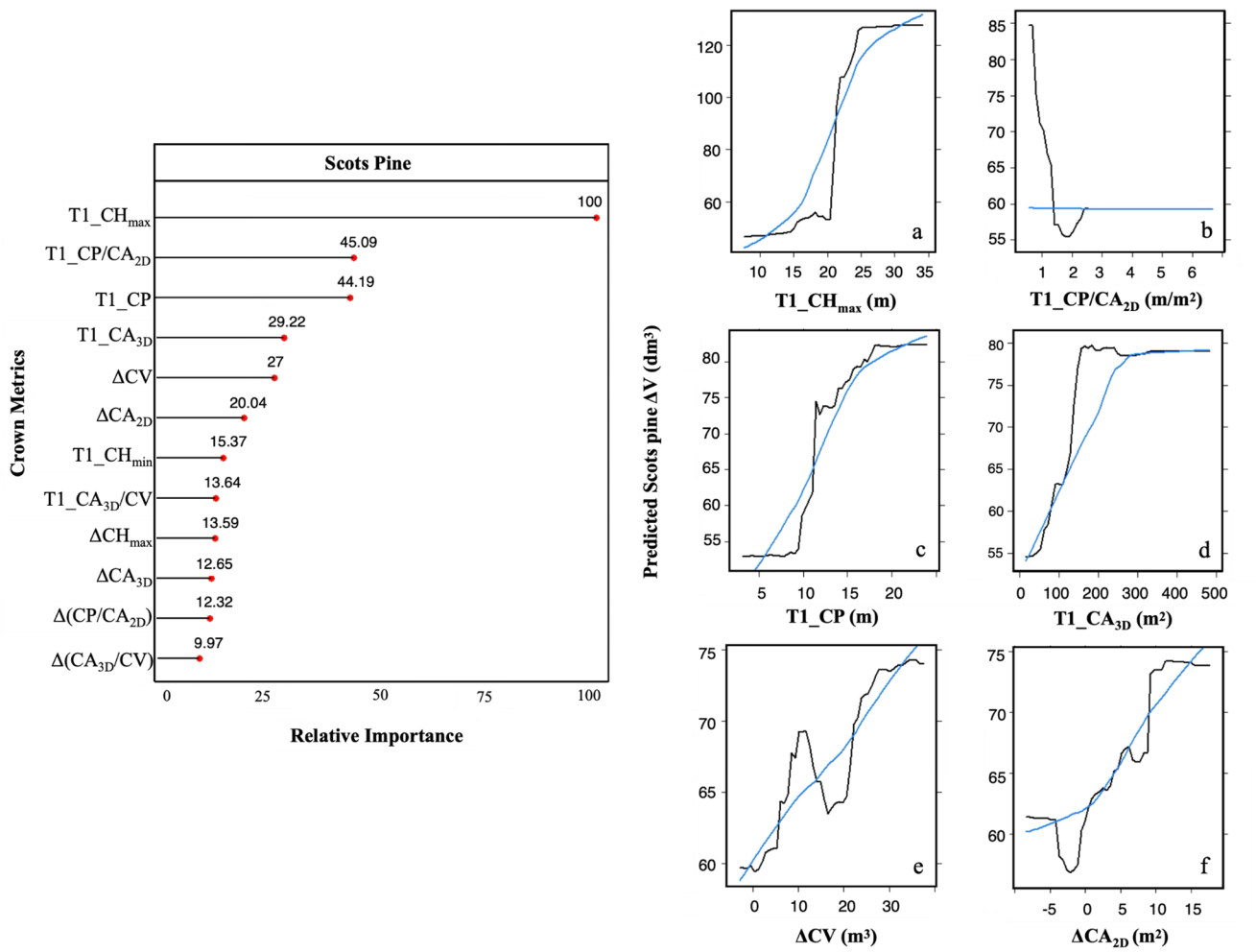

Fig. 8 Relative importance of predictors (left) characterizing the crown structure in T1 (T1_C, measured in 2014) and their changes over a 7-year time interval (ΔC) in determining individual tree stem volume growth (ΔV) for Scots pine. Partial dependence plots (right) show the effects of the most influential predictors on the predicted Scots pine ΔV (black line) and the corresponding smoothed trend (blue line)

T1_CV and ΔCA_{3D}, with relative importance values of 86.46 and 77.28 respectively, impact spruce ΔV predictions. An increase in these metrics leads to an increase in predicted ΔV as shown in Fig. 9b and c. However, it should be noted that the predicted ΔV was associated with both positive but also negative values for ΔCA_{3D} which could be attributed to challenges in correctly delineating individual tree crowns and estimating CA_{3D} using 3D convex hulls, making it a possibly unstable predictor. The predicted ΔV of Norway spruce also increased rapidly with increasing T1_CH_{max} and T1_CH_{min} (Fig. 9d and e). In contrast, a decreasing trend was found in the relationships between T1_CA_{3D}/CV and predicted spruce ΔV in a certain threshold. However, additional changes in the ratio do not contribute to the variation in the predicted ΔV (Fig. 9f).

The relative importance of selected predictors in explaining birch ΔV is shown in Fig. 10. ΔCV was identified as the most important predictor in the RF model. As shown in Fig. 10a, the predicted ΔV of birch increased as the ΔCV increased. T1_CP emerged as the second-ranked variable in explaining birch ΔV with a relative importance of 90.44. However, it showed a more gradual effect on predicted ΔV compared to ΔCV (Fig. 10b). T1_CA_{3D} also exhibited a substantial impact on birch ΔV (relative importance of 80.17), while a lower impact was found for the T1_CV (relative importance of 75.95). The ΔCP and T1_CH_{max} were among other metrics that showed considerable impact on birch ΔV, representing an overall increasing trend (Fig. 10e and f).

Discussion

This study explored how crown metrics at the beginning of the monitoring period and their changes relate to ΔV of Scots pine, Norway spruce, and birch trees using bitemporal, multisensorial point clouds. Some initial crown metrics and

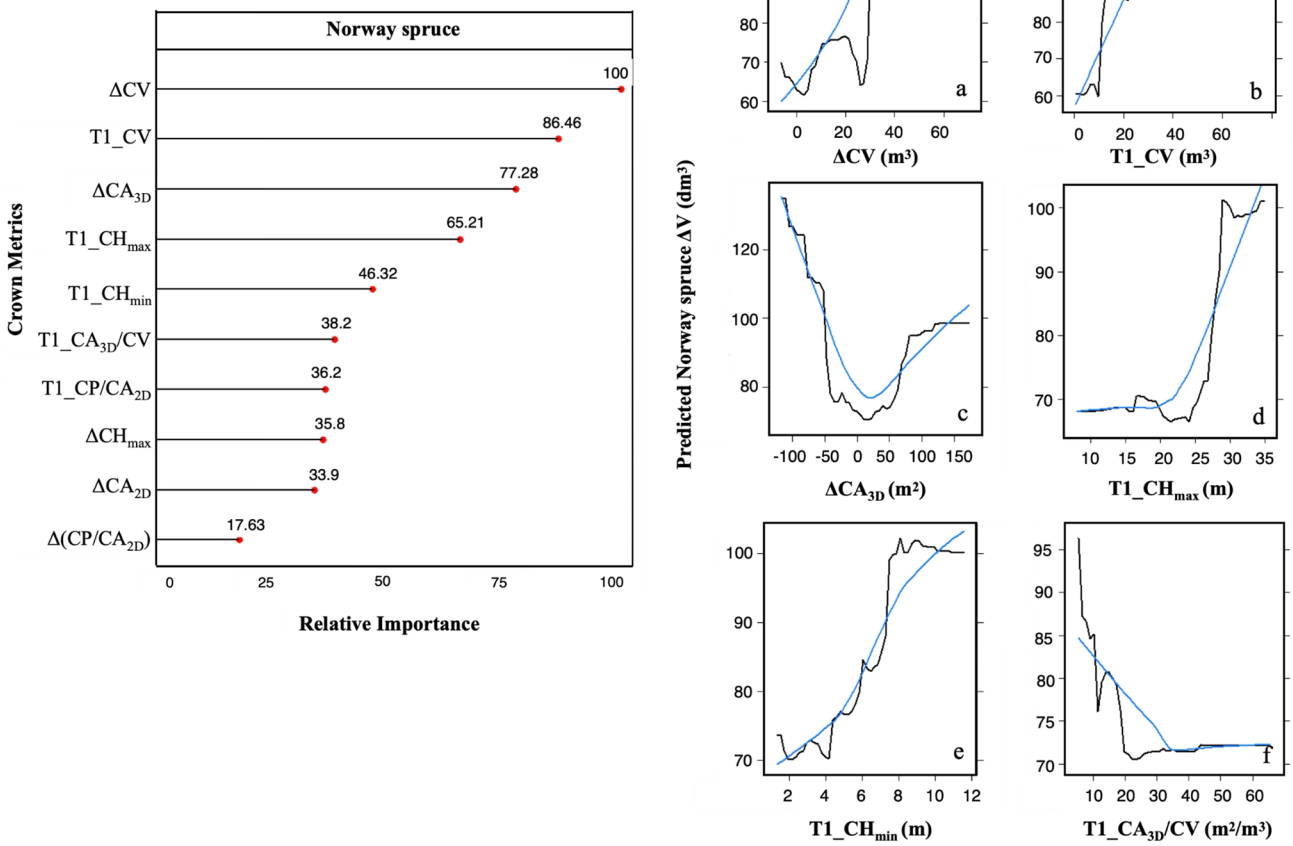

Fig. 9 Relative importance of predictors (left) characterizing the crown structure in T1 (T1_C, measured in 2014) and their changes over a 7-year time interval (ΔC) in determining individual tree stem volume growth (ΔV) for Norway spruce. Partial dependence plots (right) show the effects of the most influential predictors on the predicted Norway spruce ΔV (black line) and the corresponding smoothed trend (blue line)

their changes were significantly correlated to ΔV (Table 5), and RF models showed varying degrees of explanatory power across different tree species (Fig. 7).

Overall, crown metrics at T1 had a higher correlation with ΔV than the metrics associated with crown changes (Table 5), aligning with the results of Yrttimaa et al. (2022). It implies that a tree with larger crown initially leads to a greater increase in ΔV. Nevertheless, changes in crown metrics were relevant for Norway spruce and birch (Table 5). In particular, ΔCV and ΔCA_{3D} were among the important metrics for Norway spruce trees when RF modeling was used (Fig. 9). Similarly, changes in crown metrics such as ΔCV, ΔCP, ΔCA_{3D}, ΔCH_{min}, and $\Delta(CP/CA_{2D})$ were among the important metrics explaining birch trees ΔV (Fig. 10).

We found a strong correlation between ΔV of Scots pine and crown metrics, including T1_CV, $T1\_CA_{2D}$, T1_CP, with $T1\_CH_{max}$ also showing a notable correlation with birch ΔV (Table 5). $T1\_CH_{max}$ emerged as the most influential metric in explaining ΔV of Scots pine in RF (Fig. 8a). It was also ranked among the most important metrics for Norway spruces and birches but with lower impacts. It suggests that trees with higher $T1\_CH_{max}$ may have a competitive advantage that led to increased ΔV. T1_CP also played a substantial role in explaining ΔV for Scots pine and proved to be of high importance for the birch trees as well. According to Poorter et al. (2012), CP is one of the tree crown dimensions that allow greater access to the light. Hence, a large CP contributes to a higher level of photosynthesis and can thereby increase ΔV (Figs. 8c and 10b). Similarly, Pretzsch (2021) found that crown projection area had a strong positive effect on tree volume growth.

However, these relationships between ΔV and crown metrics are inherently complex and might vary by other factors such as stand density. For instance, CH_{max} is highly

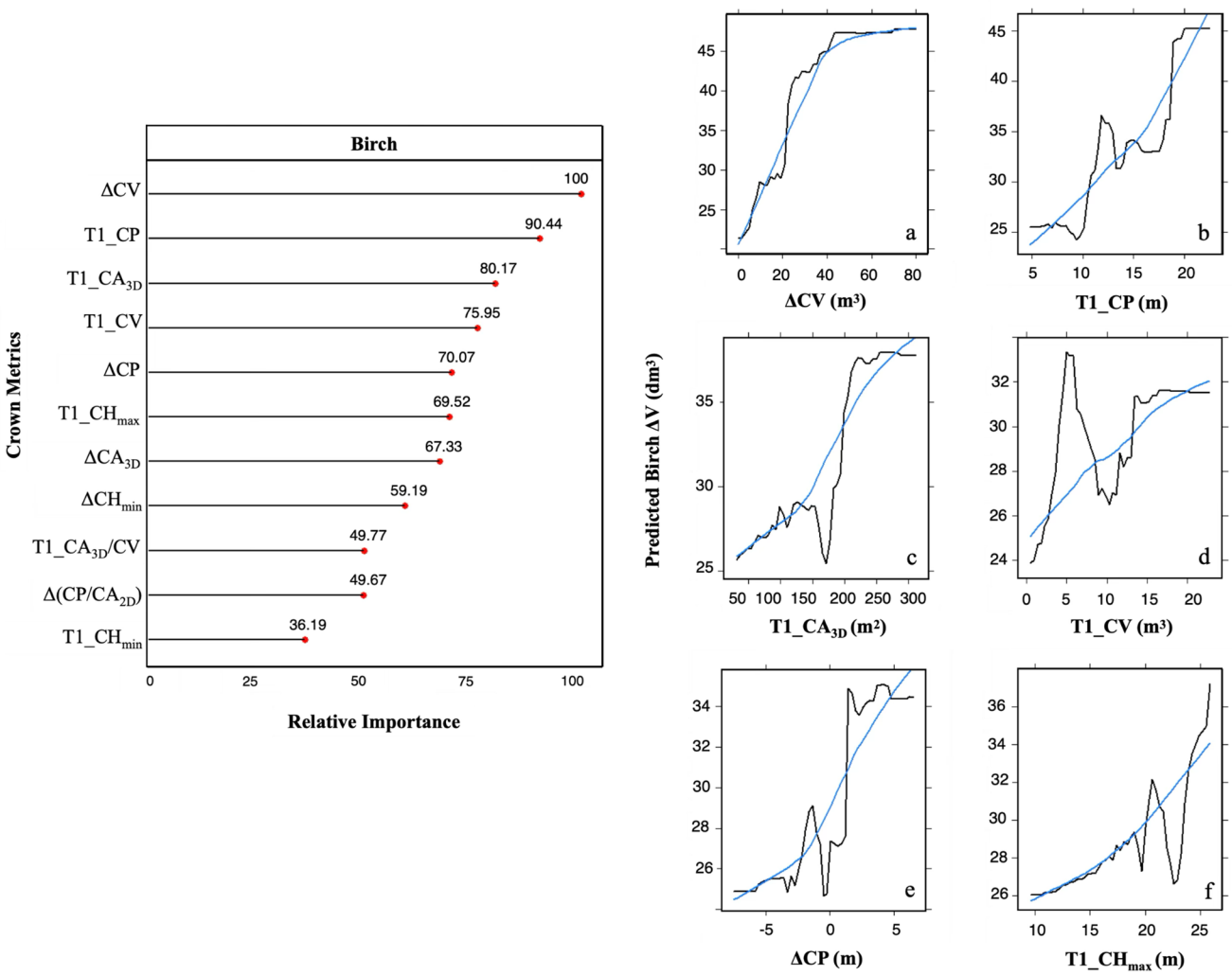

Fig. 10 Relative importance of predictors (left) characterizing the crown structure in T1 (T1_C, measured in 2014) and their changes over a 7-year time interval (ΔC) in determining individual tree stem volume growth (ΔV) for birch. Partial dependence plots (right) show the effects of the most influential predictors on the predicted birch ΔV (black line) and the corresponding smoothed trend (blue line)

affected by stand density, and constrained crown size due to high stand density could affect the growth rate of the entire tree (Valentine et al. 2012).

Unlike pine trees, Norway spruce ΔV exhibited the highest correlations with 3D crown metrics, including T1_CV, $T1\_CA_{3D}$/CV, and ΔCV (Table 5). ΔCV, T1_CV, and ΔCA_{3D} were also the metrics with high relative importance in the RF model explaining Norway spruce ΔV. An increase in these metrics was generally associated with higher predicted ΔV for Norway spruce (Fig. 9a, b, and c). Moreover, $T1\_CH_{min}$ in Norway spruce was also among the most correlated metrics with ΔV and showed relatively high importance in the RF model (Table 5; Fig. 9). This is in line with the findings by Yrttimaa et al. (2022) in a similar study utilizing TLS in the boreal forest. They identified the strongest relationship for Norway spruce, associating CH_{min} to ΔV with an R^2 of 0.52. CH_{min} can be related to the length of clear bole, which was important metric in profile theory of growth proposed by Osawa et al. (1991). This theory provides a framework for understanding how the stem mass density at the crown base can influence the growth of an entire tree. They developed a model that explains the above-mentioned relationship under specific assumptions such as vertical foliage distribution and constant annual height growth. The model successfully predicted tree growth patterns across different tree species by incorporating other metrics such as height growth, foliage mass, and length of clear bole. There is, however, uncertainty in defining the CH_{min} in our study due to the inaccuracy in the classification of points into stem and crown, the presence of neighbors in the tree's branch architecture, and imputed values for the trees that CH_{min} couldn't be directly defined. $T1\_CH_{min}$ was also not featured as a highly ranked metric for explaining Scots pine ΔV (Fig. 8), while previous research has shown the variation in CH_{min}

driven by stand density can affect stem growth (Beekhuis 1965; Fish et al. 2006; Mäkelä and Valentine 2006). For birch, we did not observe the same level of importance for $T1\_CH_{min}$. However, given the small sample size of birch trees ($n = 77$), it is important to interpret this finding with caution. Moreover, our data were mostly collected during the leaf-off conditions, likely resulting in an underestimation of the crown characteristics of the birch trees.

It is worth mentioning that we used RF modeling and the Gini index to better understand the relationship between ΔV and crown structural metrics at both T1 and their changes over time, rather than to build a predictive model. RF models are highly flexible in a wide range of data types without requiring a pre-specified functional form for relationships. They can capture complex data patterns and interactions (Breiman 2001), making them robust for our analysis. In addition, we complemented RF with partial dependence plots to enhance model interpretability, illustrating how the variability of key predictors affects the variability of ΔV. Given that the models were fitted on the full dataset, their predictive performance and generalizability cannot be assessed, but they give insight into relative importance of metrics within the observed data.

The observed dependencies between ΔV and crown metrics varied between different tree species (Fig. 7), although it might represent dynamics that differ from those over a longer time frame. Additionally, growth allocation may vary based on internal tree characteristics and stem itself beyond the crown structure (Pretzsch 2020) which hasn't been considered in our study. The site conditions, provenance, tree age, and mean tree size of the stand can also affect the observed relationships (Pretzsch et al. 2022). However, individual tree characteristics are particularly more relevant to ΔV in heterogeneous stands where trees vary strongly in social status, crown structure, and growth (Pretzsch and Rais 2016; Pretzsch 2019). For example, Pretzsch (2021), used linear regression models to understand how stem volume growth is influenced by internal, structural, and morphological characteristics of trees in monospecific stands of different species. Their prediction model for volume growth, with stem volume as a predictor, resulted in an RMSE of 0.67 $m^3 year^{-1}$. The inclusion of tree age, mean tree volume, crown projection area, crown ratio, and mean tree ring width reduced the RMSE by up to 43%. Many of these attributes can be obtained with our approach and it could be utilized in assessing their effects on ΔV in future research. Furthermore, more research is needed on how multisensorial point clouds can provide information for studying the growth allocation of different tree species.

In this study, we used a multisensorial dataset with top- and below-viewpoints that was assumed to fill the gap caused by occlusion within a crown segment and potentially reduce the error related to metric estimations (Panagiotidis et al. 2022). Point density is another factor strongly affecting the accuracy of the extracted CHM and the metrics such as height (Zhao et al. 2018). Hence, the high-density point clouds used in this study suppressed the limitations associated with lower-density data. However, it is important to acknowledge the specific constraints associated with the point cloud measurements in this study. While Marker-controlled watershed segmentation is known as an effective algorithm for tree crown delineation, it is likely prone to over- and under-segmentation and omits small trees with crowns mixed with their taller neighbors (Kwak et al. 2007). It is therefore important to note that after applying the CHM-based tree segmentation, we searched for possible cases where multiple trees were found inside the segments and further partitioned the segment accordingly. Despite these efforts, we acknowledge the possibility of inaccurate tree crown segmentation, particularly in the analysis of the crown dimensions over different time points. This could have influenced the consistency of the crown metrics derived at two time points. However, the observed disparities are confounded with both errors and inherent dynamics of tree crowns. The co-registration accuracy between the terrestrial and aerial point clouds and the discrepancy in the used methods at T1 and T2 also may have affected the results. This could have led to a spatial mismatch between the trees identified at T1 and T2 that could have decreased the reliability of the tree-to-tree matching. Moreover, it may have affected the number of trees that were correctly linked to the field-measure trees from which tree species information was derived. The GNSS errors at T1 and the limited capacity of the applied co-registration methods at T2 to provide accurate transformation information can potentially cause co-registration inaccuracy. Point cloud analysis may also be influenced by differences between sensors, sampling designs, and resulting point cloud properties at different time points (Cao et al. 2016; Socha et al. 2017; Zhao et al. 2018). The TLS field of view and the number and positions of scans might also have resulted in occlusion and thereby spatial mismatches. Negative observations in ΔV, which were likely attributed to occlusion and the inaccurate taper curve estimation, posed an additional challenge in the analysis and interpretation of this study. Especially, it occurs when the magnitude of the actual change falls within the accuracy limits of the measurement technique. Accordingly, understanding the time interval to overcome excess noises and reveal real patterns can be crucial in forest change detection, particularly in slow-growth boreal forests (Yu et al. 2006; Coops 2015; Socha et al. 2017). Considering the continuous improvement in the segmentation algorithms in accuracy and efficiency and the growing availability of TLS measurements, our multisensorial approach is expected to become

more popular in small-scale ecological studies that require a more comprehensive representation of tree crowns.

Conclusion

In this study, we showed that the relationship between stem volume growth (ΔV) and crown metrics at the beginning of the monitoring period (T1_C) as well as their changes over time (ΔC) can be captured with bi-temporal, multisensorial point clouds. The data included TLS and high-density ALS acquired in 2014 (T1) and 2021 (T2), covering plots dominated by Scots pine, Norway spruce, and birch trees. We observed consistent measurements in T1 and T2, despite notable variation in certain crown metrics which may limit the ability to discern subtle changes from measurement errors. Crown structural metrics in T1 showed overall stronger correlation with species-specific ΔV compared to ΔC-related metrics. Nevertheless, the RF analyses indicated that ΔCV and ΔCA_{3D} were determining metrics for birch and Norway spruce trees. Thus, it can be concluded that the relationship between ΔV and crown metrics varied between species, even though some similarities were observed. Crown metrics at T1 and their changes over time accounted for 50% of the variation in ΔV of Scots pine while explaining 20% and 6% of the variation in ΔV for Norway spruce and birch trees, respectively. Our results can support the design of forest monitoring plots and future large-scale assessments of forest growth. Forest monitoring plots are used for understanding tree growth and our approach can be used for that, also with detailed data from drones, for example. In the long term, advances in ALS technology could enable the collection of detailed point clouds over large areas at lower costs, allowing changes in individual tree crowns to be linked with stem volume growth. However, such data remains costly, and large-scale operational applications may still take time to become feasible.

Author contributions M.P. Formal analysis, Investigation, Methodology, Software, Validation, Visualization, Writing–original draft. G.R. Formal analysis, Writing—review & editing. T.Y. Investigation, Methodology, Software, Writing—review & editing. V.L. Data curation. S.B. Writing—review & editing. S.H. Writing—review & editing. J.H. Funding acquisition, Resources. N.S. Supervision, Writing—review & editing. V.K. Conceptualization, Investigation, Supervision, Writing—review & editing. M.V. Conceptualization, Funding acquisition, Project administration, Resources, Supervision, Writing—review & editing.

Funding Open access funding provided by University of Eastern Finland (including Kuopio University Hospital). This study was funded by the Research Council of Finland through Forest–Human–Machine Interplay Flagship of Science (decision number 337127), Understanding Wood Density Variation Within and Between Trees Using Multispectral Point Cloud Technologies and X-ray microdensitometry project (decision number 331711), and Measuring Spatiotemporal Changes in Forest Ecosystem Research Infrastructure (decision numbers 337810 and 346383).

Data availability Data can be available on request.

Declarations

Conflict of interest The authors declare no competing interests.

References

Beekhuis J (1965) Crown depth of radiata pine in relation to stand density. New Zeal J for 10:43–61

Breiman L (2001) Random forests. Mach Learn 45:5–32

Calders K, Adams J, Armston J et al (2020) Terrestrial laser scanning in forest ecology: expanding the horizon. Remote Sens Environ 251:112102. https://doi.org/10.1016/J.RSE.2020.112102

Cao L, Coops NC, Innes JL et al (2016) Estimation of forest biomass dynamics in subtropical forests using multi-temporal airborne lidar data. Remote Sens Environ 178:158–171. https://doi.org/10.1016/j.rse.2016.03.012

Coomes DA, Allen RB (2007) Effects of size, competition and altitude on tree growth. J Ecol 95:1084–1097. https://doi.org/10.1111/j.1365-2745.2007.01280.x

Coops NC (2015) Characterizing forest growth and productivity using remotely sensed data. Curr Rep 1:195–205. https://doi.org/10.1007/s40725-015-0020-x

Dai W, Yang B, Liang X et al (2019) Automated fusion of forest airborne and terrestrial point clouds through canopy density analysis. ISPRS J Photogramm Remote Sens 156:94–107. https://doi.org/10.1016/J.ISPRSJPRS.2019.08.008

Enquist BJ, West GB, Brown JH (2009) Extensions and evaluations of a general quantitative theory of forest structure and dynamics. Proc Natl Acad Sci U S A 106:7046–7051. https://doi.org/10.1073/pnas.0812303106

Fernández-Sarría A, Martínez L, Velázquez-Martí B et al (2013) Different methodologies for calculating crown volumes of Platanus Hispanica trees using terrestrial laser scanner and a comparison with classical dendrometric measurements. Comput Electron Agric 90:176–185. https://doi.org/10.1016/J.COMPAG.2012.09.017

Fish H, Lieffers VJ, Silins U, Hall RJ (2006) Crown shyness in lodgepole pine stands of varying stand height, density, and site index in the upper foothills of Alberta. Can J Res 36:2104–2111. https://doi.org/10.1139/X06-107

Franklin JF, Spies TA, Pelt R, Van et al (2002) Disturbances and structural development of natural forest ecosystems with silvicultural implications, using Douglas-fir forests as an example. Ecol

Manage 155:399–423. https://doi.org/10.1016/S0378-1127(01)00575-8
Fraver S, D'Amato AW, Bradford JB et al (2014) Tree growth and competition in an old-growth Picea abies forest of boreal sweden: influence of tree Spatial patterning. J Veg Sci 25:374–385. https://doi.org/10.1111/jvs.12096
Greenwell BM (2017) Pdp: an R package for constructing partial dependence plots. R J 9:421–436. https://doi.org/10.32614/rj-2017-016
Hapfelmeier A, Hothorn T, Ulm K, Strobl C (2014) A new variable importance measure for random forests with missing data. Stat Comput 24:21–34. https://doi.org/10.1007/S11222-012-9349-1/FIGURES/8
Harja D, Vincent G, Mulia R, van Noordwijk M (2012) Tree shape plasticity in relation to crown exposure. Trees Struct Funct 26:1275–1285. https://doi.org/10.1007/S00468-012-0703-X/TABLES/6
Jung SE, Kwak DA, Park T et al (2011) Estimating Crown Variables of Individual Trees Using Airborne and Terrestrial Laser Scanners. Remote Sens 3:2346–2363. https://doi.org/10.3390/RS3112346
Kankare V, Vauhkonen J, Tanhuanpää T et al (2014) Accuracy in Estimation of timber assortments and stem distribution–A comparison of airborne and terrestrial laser scanning techniques. ISPRS J Photogramm Remote Sens 97:89–97
Kwak DA, Lee WK, Lee JH et al (2007) Detection of individual trees and Estimation of tree height using lidar data. J Res 12:425–434. https://doi.org/10.1007/s10310-007-0041-9
Laasasenaho J (1982) Taper curve and volume functions for pine, spruce and birch. Metsäntutkimuslaitos
Liang X, Kankare V, Yu X et al (2014) Automated stem curve measurement using terrestrial laser scanning. IEEE Trans Geosci Remote Sens 52:1739–1748. https://doi.org/10.1109/TGRS.2013.2253783
Liang X, Hyyppä J, Kaartinen H et al (2018) International benchmarking of terrestrial laser scanning approaches for forest inventories. ISPRS J Photogramm Remote Sens 144:137–179. https://doi.org/10.1016/J.ISPRSJPRS.2018.06.021
Liu G, Wang J, Dong P et al (2018) Estimating individual tree height and diameter at breast height (DBH) from terrestrial laser scanning (TLS) data at plot level. Forests 9:398
Luoma V, Saarinen N, Wulder MA et al (2017) Assessing precision in conventional field measurements of individual tree attributes. Forests 8:38. https://doi.org/10.3390/f8020038
Luoma V, Yrttimaa T, Kankare V et al (2021) Revealing changes in the stem form and volume allocation in diverse boreal forests using two-date terrestrial laser scanning. Forests 12:835
Lüttge U, Hertel B (2009) Diurnal and annual rhythms in trees. Trees Struct Funct 23:683–700. https://doi.org/10.1007/S00468-009-0324-1/FIGURES/7
Mäkelä A, Valentine HT (2006) Crown ratio influences allometric scaling in trees. Ecology 87:2967–2972. https://doi.org/10.1890/0012-9658(2006)87[2967:CRIASI]2.0.CO;2
Metz JÔ, Seidel D, Schall P et al (2013) Crown modeling by terrestrial laser scanning as an approach to assess the effect of aboveground intra- and interspecific competition on tree growth. Ecol Manage 310:275–288. https://doi.org/10.1016/J.FORECO.2013.08.014
Meyer F, Beucher S (1990) Morphological segmentation. J Vis Commun Image Represent 1:21–46. https://doi.org/10.1016/1047-3203(90)90014-M
Muller-Landau HC, Condit RS, Chave J et al (2006) Testing metabolic ecology theory for allometric scaling of tree size, growth and mortality in tropical forests. Ecol Lett 9:575–588. https://doi.org/10.1111/J.1461-0248.2006.00904.X
Niklas KJ (1994) Plant allometry: the scaling of form and process. University of Chicago Press
Osawa A, Ishizuka M, Kanazawa Y (1991) A profile theory of tree growth. Ecol Manage 41:33–63. https://doi.org/10.1016/0378-1127(91)90118-F
Ottorini J-M, Goff N, Le, Cluzeau C (1996) Relationships between crown dimensions and stem development in fraxinus excelsior. Can J Res 26:394–401
Panagiotidis D, Abdollahnejad A, Slavík M (2022) 3D point cloud fusion from UAV and TLS to assess temperate managed forest structures. Int J Appl Earth Obs Geoinf 112:102917. https://doi.org/10.1016/J.JAG.2022.102917
Pitkänen J, Maltamo M, Hyyppä J, Yu X (2004) Adaptive methods for individual tree detection on airborne laser based canopy height model. Nternational Arch Photogramm Remote Sens Spat Inf Sci 36:187–191
Poorter L, Lianes E, Moreno-de las Heras M, Zavala MA (2012) Architecture of Iberian canopy tree species in relation to wood density, shade tolerance and climate. Plant Ecol 213:707–722. https://doi.org/10.1007/s11258-012-0032-6
Popescu SC, Wynne RH (2004) Seeing the trees in the forest: using lidar and multispectral data fusion with local filtering and variable window size for estimating tree height. Photogramm Eng Remote Sens 70:589–604. https://doi.org/10.14358/PERS.70.5.589
Pretzsch H (2009) Growing space and competitive situation of individual trees. Forest dynamics, growth and yield: from measurement to model. Berlin, Heidelberg: Springer Berlin Heidelberg, pp 291–336. https://doi.org/10.1007/978-3-540-88307-4_8
Pretzsch H (2019) The effect of tree crown allometry on community dynamics in mixed-species stands versus monocultures. A review and perspectives for modeling and silvicultural regulation. Forests 10:810. https://doi.org/10.3390/f10090810
Pretzsch H (2020) The course of tree growth. Theory and reality. Ecol Manage 478:118508. https://doi.org/10.1016/J.FORECO.2020.118508
Pretzsch H (2021) Tree growth as affected by stem and crown structure. Trees - Struct Funct 35:947–960. https://doi.org/10.1007/S00468-021-02092-0/FIGURES/5
Pretzsch H, Rais A (2016) Wood quality in complex forests versus even-aged monocultures: review and perspectives. Wood Sci Technol 50:845–880. https://doi.org/10.1007/s00226-016-0827-z
Pretzsch H, Forrester DI, Rötzer T (2015) Representation of species mixing in forest growth models. A review and perspective. Ecol Modell 313:276–292. https://doi.org/10.1016/J.ECOLMODEL.2015.06.044
Pretzsch H, Ahmed S, Jacobs M et al (2022) Linking crown structure with tree ring pattern: methodological considerations and proof of concept. Trees Struct Funct 36:1349–1367. https://doi.org/10.1007/s00468-022-02297-x
Rapidlasso (2023) Rapidlasso. https://rapidlasso.com
Saarinen N, Kankare V, Vastaranta M et al (2017) Feasibility of terrestrial laser scanning for collecting stem volume information from single trees. ISPRS J Photogramm Remote Sens 123:140–158
Schneider FD, Kükenbrink D, Schaepman ME et al (2019) Quantifying 3D structure and occlusion in dense tropical and temperate forests using close-range lidar. Agric Meteorol 268:249–257. https://doi.org/10.1016/J.AGRFORMET.2019.01.033
Seidel D, Annighöfer P, Stiers M et al (2019) How a measure of tree structural complexity relates to architectural benefit-to-cost ratio, light availability, and growth of trees. Ecol Evol 9:7134–7142. https://doi.org/10.1002/ece3.5281
Sheppard J, Morhart C, Hackenberg J, Spiecker H (2017) Terrestrial laser scanning as a tool for assessing tree growth. iForest Biogeosciences for 10:172–179
Socha J, Pierzchalski M, Bałazy R, Ciesielski M (2017) Modelling top height growth and site index using repeated laser scanning data.

Ecol Manage 406:307–317. https://doi.org/10.1016/J.FORECO.2017.09.039
Srinivasan S, Popescu SC, Eriksson M et al (2014) Multi-temporal terrestrial laser scanning for modeling tree biomass change. Ecol Manage 318:304–317. https://doi.org/10.1016/J.FORECO.2014.01.038
Srinivasan S, Popescu SC, Eriksson M et al (2015) Terrestrial laser scanning as an effective tool to retrieve tree level height, crown width, and stem diameter. Remote Sens 7:1877–1896
Terryn L, Calders K, Bartholomeus H et al (2022) Quantifying tropical forest structure through terrestrial and UAV laser scanning fusion in Australian rainforests. Remote Sens Environ 271:112912. https://doi.org/10.1016/J.RSE.2022.112912
Vaglio Laurin G, Ding J, Disney M et al (2019) Tree height in tropical forest as measured by different ground, proximal, and remote sensing instruments, and impacts on above ground biomass estimates. Int J Appl Earth Obs Geoinf 82:101899. https://doi.org/10.1016/J.JAG.2019.101899
Valentine HT, Mäkelä A, Green EJ et al (2012) Models relating stem growth to crown length dynamics: application to loblolly pine and Norway Spruce. Trees - Struct Funct 26:469–478. https://doi.org/10.1007/S00468-011-0608-0/FIGURES/7
Vastaranta M, Melkas T, Holopainen M et al (2009) Laser-based field measurements in tree-level forest data acquisition. Photogramm J Finl 21:51–61
Vincent G, Harja D (2008) Exploring ecological significance of tree crown plasticity through Three-dimensional modelling. Ann Bot 101:1221–1231. https://doi.org/10.1093/AOB/MCM189
Weiner J (1990) Asymmetric competition in plant populations. Trends Ecol Evol 5:360–364. https://doi.org/10.1016/0169-5347(90)90095-U
Weiner J (2004a) Allocation, plasticity and allometry in plants. Perspect Plant Ecol Evol Syst 6:207–215. https://doi.org/10.1078/1433-8319-00083
Weiner J (2004b) Allocation, plasticity and allometry in plants. Perspect Plant Ecol Evol Syst 6:207–215. https://doi.org/10.1078/1433-8319-00083
Weiskittel AR, Hann DW, Kershaw JA, Vanclay JK (2011) Forest Growth and Yield Modeling. For Growth Yield Model. https://doi.org/10.1002/9781119998518
Yan Z, Liu R, Cheng L et al (2019) A concave hull methodology for calculating the crown volume of individual trees based on vehicle-borne lidar data. Remote Sens 11:623
Yrttimaa T, Saarinen N, Kankare V et al (2019) Investigating the feasibility of multi-scan terrestrial laser scanning to characterize tree communities in Southern boreal forests. Remote Sens 11:1423
Yrttimaa T, Saarinen N, Kankare V et al (2020a) Performance of terrestrial laser scanning to characterize managed Scots pine (Pinus sylvestris L.) stands is dependent on forest structural variation. ISPRS J Photogramm Remote Sens 168:277–287. https://doi.org/10.1016/J.ISPRSJPRS.2020.08.017
Yrttimaa T, Saarinen N, Kankare V et al (2020b) Multisensorial close-range sensing generates benefits for characterization of managed Scots pine (Pinus sylvestris L.) stands. ISPRS Int J Geo-Information 9:309. https://doi.org/10.3390/ijgi9050309
Yrttimaa T, Luoma V, Saarinen N et al (2022) Exploring tree growth allometry using two-date terrestrial laser scanning. Ecol Manage 518:120303. https://doi.org/10.1016/J.FORECO.2022.120303
Yu X, Hyyppä J, Kukko A et al (2006) Change detection techniques for canopy height growth measurements using airborne laser scanner data. Photogramm Eng Remote Sens 72:1339–1348. https://doi.org/10.14358/PERS.72.12.1339
Yun T, Cao L, An F et al (2019) Simulation of multi-platform lidar for assessing total leaf area in tree crowns. Agric Meteorol 276–277:107610. https://doi.org/10.1016/J.AGRFORMET.2019.06.009
Zhang Z (1994) Iterative point matching for registration of free-form curves and surfaces. Int J Comput Vis 13:119–152. https://doi.org/10.1007/BF01427149/METRICS
Zhao K, Suarez JC, Garcia M et al (2018) Utility of multitemporal lidar for forest and carbon monitoring: tree growth, biomass dynamics, and carbon flux. Remote Sens Environ 204:883–897. https://doi.org/10.1016/j.rse.2017.09.007

Authors and Affiliations

Maryam Poorazimy[1] · Ghasem Ronoud[1,2] · Tuomas Yrttimaa[1] · Ville Luoma[3] · Simone Bianchi[4] · Saija Huuskonen[4,5] · Juha Hyyppä[6] · Ninni Saarinen[1] · Ville Kankare[6,7] · Mikko Vastaranta[1]

✉ Maryam Poorazimy
maryam.poorazimy@uef.fi

Ghasem Ronoud
ghasem.ronoud@oulu.fi

Tuomas Yrttimaa
tuomas.yrttimaa@uef.fi

Ville Luoma
ville.luoma@helsinki.fi

Simone Bianchi
simone.bianchi@luke.fi

Saija Huuskonen
saija.huuskonen@metsa.fi

Juha Hyyppä
juha.hyyppa@nls.fi

Ninni Saarinen
ninni.saarinen@uef.fi

Ville Kankare
viveka@utu.fi

Mikko Vastaranta
mikko.vastaranta@uef.fi

[1] School of Forest Sciences, University of Eastern Finland, 80101 Joensuu, Finland

[2] Ecology and Genetics Research Unit, University of Oulu, 90014 Oulu, Finland

[3] Department of Forest Sciences, University of Helsinki, 00790 Helsinki, Finland

[4] Natural Resources Institute Finland, 00790 Helsinki, Finland

[5] Metsähallitus Forestry Ltd, 00520 Helsinki, Finland

[6] Department of Photogrammetry and Remote Sensing, Finnish Geospatial Research Institute FGI, National Land Survey of Finland, 02150 Espoo, Finland

[7] Department of Geography and Geology, University of Turku, 20014 Turku, Finland